PHYSICAL REVIEW A VOLUME 18, NUMBER 2 AUGUST 1978

$H + N_2$ and $H + O_2$ collisions: Experimental charge-production cross sections and differential scattering calculations

B. Van Zyl, H. Neumann, T. Q. Le, and R. C. Amme
Department of Physics, University of Denver, Denver, Colorado 80208
(Received 11 October 1977)

Absolute total cross sections for producing H^+, H^-, e^-, N_2^+, and O_2^+ have been measured for $H + N_2$ and $H + O_2$ collisions from 50-eV to 3-keV hydrogen-atom energy. The experimental techniques used, when combined with classical differential-scattering calculations, also allowed determinations of the absolute large-angle-scattering differential cross sections for H^+ production. The experimental and theoretical procedures are reviewed, and the results are compared, where possible, with the data of other investigators.

I. INTRODUCTION

This paper presents the results of a series of measurements of cross sections for production of various charged collision products resulting from hydrogen-atom scattering from N_2 and O_2 molecules. Specifically, for N_2 targets, the reactions investigated are

$$H + N_2 \rightarrow H^+ + e^- + N_2 , \quad (1)$$

$$H + N_2 \rightarrow H + e^- + N_2^+ , \quad (2)$$

$$H + N_2 \rightarrow H^- + N_2^+ . \quad (3)$$

The product molecules or molecular ions from these reactions could be dissociated, as no provision was made to identify the slow-product species.

For the case of O_2 targets, the same reactions were investigated with the exception that the e^- and O_2 products of reaction (1) could leave the collision in a bound O_2^- (or dissociated $O + O^-$) configuration. Again, this experiment did not distinguish these possibilities.

The proton-production (ionization-stripping) cross section σ_{01} is defined by reaction (1). Similarly, reaction (3) defines the σ_{0-1} cross section. The N_2^+ formation cross section $\sigma_{N_2^+}$ represents the sum of reactions (2) and (3). Finally, the total charge-production cross sections σ_t^- and σ_t^+, for negative and positive charge, respectively, are the sums of all three reactions. These cross sections, which obviously must be identical, are nevertheless distinguished here as each has been individually measured.

The techniques used to make the measurements of these cross sections and the motivations for such studies are described in a previous paper, where the results of similar determinations for $H + Ar$ collisions are presented in detail.[1] This earlier paper also shows how, by using a more complex scattering-cell arrangement than had previously been employed for such ionization studies, information could be obtained which, combined with classical scattering calculations,[2] yields the absolute differential cross section for proton formation.

Since the procedures used in making the studies reported here are similar to those used for Ar targets, the experimental details are only briefly reviewed in Sec. II. The differential-scattering calculations, however, require some additional attention to outline how they were extended to include scattering from molecular targets. The techniques used are described in Sec. III, as are the results of the differential cross-section determinations. The results of the total cross-section measurements are discussed in Sec. IV, where they are compared with the data of other workers, generally obtained at collision energies above those of primary interest here (the region below 1 keV energy). A brief discussion of all results is given in Sec. V.

II. BASIC EXPERIMENTAL PROCEDURE

The technique used in this work for generating the fast hydrogen-atom beam involves photodetaching electrons from negative hydrogen ions. The H^- ions, extracted from a duoplasmatron source, were mass analyzed and focused into a parallel or slightly converging beam on the order of 1 mm diameter.[3] This beam was directed through the cavity of an yttrium aluminum garnet laser (1064 nm) whose end mirrors are totally reflecting. The photodetaching reaction

$$H^- + h\nu \rightarrow H + e^- , \quad (4)$$

proceeds with an efficiency such that several percent of the H^- ions were neutralized in the energy range of interest.[4] The details of this procedure are presented elsewhere[5] and will not be reviewed here. It should be noted, however, that the technique leads to production of an intense neutral beam upon which stringent conditions of direct-

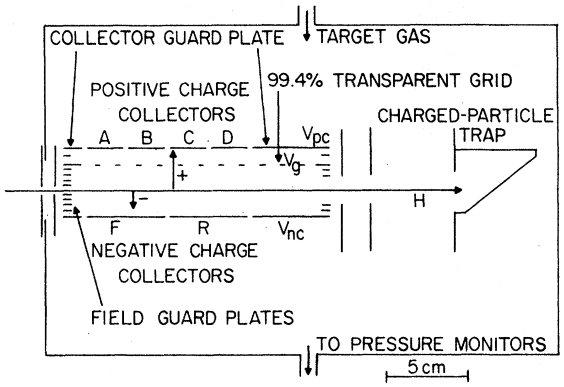

FIG. 1. Target cell and charged-particle detectors.

ionality and divergence can be imposed, and whose absolute flux intensity can be determined to within a net uncertainty of ±3% (Ref. 6).

This energy-selected and highly collimated H-atom beam enters the target scattering cell, shown schematically in Fig. 1, through two 5-mm-diameter differential pumping apertures. During each cross-section measurement, the pressure (typically 1 to 3×10^{-4} Torr) was monitored with a Bayard-Alpert ionization gauge. Before and after such periods, the gauge was calibrated against a capacitance diaphragm manometer which was in turn calibrated against an absolute micrometer-point contact manometer of the type described by Ruthberg.[7] The capacitance manometer linearity between these pressure ranges was demonstrated[8] to within ±2.1%. This value was combined (in quadrature) with others associated with the pressure and temperature measurements to give a net uncertainty of ±6% for the target-gas-density determination.

The basic charged-particle detector (Fig. 1) is an elaborate version of the parallel-plate ionization chamber first employed by Utterback and Miller.[9] In general, the grid potential V_g in such devices must be kept negative relative to all collector surfaces to suppress secondary electron emission. For collecting negative collision products, the negative-charge collectors are used (with $V_{nc}=0$), V_g is typically a few hundred volts negative, and V_{pc} is about 0.6 V_g. Electrons and negative ions produced by ionizing collisions along the beam path are driven to the negative-charge collectors by the negative V_g where their current signal is measured. For positive-ion collection, the positive-charge collectors are used (with $V_{pc}=0$). For typical values like $V_g=-15$ V and $V_{nc}=+75$ V, the potential along the entering beam axis is about +30 V, causing the positive ions to be accelerated towards and pass through the highly transparent grid (99.4% at normal incidence) and reach the positive-charge collectors.

Figure 1 shows that four positive-charge collectors (i.e., A, B, C, and D) were used. This feature was incorporated to allow separation of the signals from the slow positive target ions and the large-angle-scattered protons. Thus, the measured signal to collector B, for example, can be written

$$S^+_{mB} = S_{N_2^+} + B_h N_t \int_0^X \left[\int_{\Delta\Omega_B(x,\theta,\phi,V)} F(x,\theta) \times \left(\frac{d\sigma_{01}}{d\Omega}\right) d\Omega \right] dx , \quad (5)$$

where $S_{N_2^+}$ is the slow target ion signal (the same to all four collectors, under the "thin target" conditions of the experiment) and the second term is the contribution from scattered protons. This second term involves an integration of the differential proton-production cross section $d\sigma_{01}/d\Omega$ over the solid angle $\Delta\Omega_B(x,\theta,\phi,V)$ from each point x along the beam path from which a proton, produced at scattering angle θ and azimuth ϕ, can reach collector B under the influence of target cell potentials V. The factor $F(x,\theta)$ accounts for the target-gas density gradient near the cell entrance and some geometrical restrictions on the proton orbits.

It can be shown[1] that, if only the angular dependence of $d\sigma_{01}/d\Omega$ (as opposed to its absolute value as well) were known, by taking ratios of the scattered proton signals to various pairs of the four collectors, the absolute magnitudes of both $S_{N_2^+}$ and the second term of Eq. (5) can be determined. In this work, the angular dependence of $d\sigma_{01}/d\Omega$ is assumed to be the same as that of $d\sigma_e/d\Omega$, the differential cross section for elastic scattering, which is in turn obtained from classical scattering calculations. The validity of this angular-dependence assumption can be tested by the fit of the computed second term of Eq. (5) to the measured signals to the four collectors, since rather different ranges of scattering angles prove to be important for the protons that reach the collectors. (Additional verification of this assumption, the calculational procedure for $d\sigma_e/d\Omega$, and the differential cross sections for proton production are presented in Sec. III.) Thus, explicit analysis of the scattered proton effects enabled both a determination of $d\sigma_{01}/d\Omega$ in the large-angle range, and a determination of $\sigma_{N_2^+}$ with significant improvement in accuracy.

If the collection fields for positively charged collision products are sufficiently large, it is possible to saturate the collection of both protons and slow target ions at those collectors toward the rear of the target cell. This total positive-

charge-production cross section σ_t^+ was determined here for hydrogen-atom energies below 1 keV.[10] This cross section must, of course, be identical with its σ_t^- counterpart. In the region between 0.1 and 1 keV, the average of the ratios σ_t^-/σ_t^+ was found to be 1.024 ± 0.024 (the standard deviation of the individual ratios). Such agreement between these basically independent measurements of the same cross section, taken under vastly different collection conditions and months apart in time, largely removes major concern over independent evaluation of such otherwise elusive problems as ions bouncing from collector surfaces, substantial secondary ion emission from surfaces, or improper accounting for secondary electron effects.

The presence of fast H^- ions from reaction (3) amongst the collision products was first observed in studies of the negative-charge collection efficiency as a function of grid potential V_g.[1] Such grid saturation curves exhibited structures at V_g values for which fast H^- ions, produced near the cell entrance and scattered in the forward direction, would arrive at a collector edge under the influence of the applied V_g. Thus, by using the appropriate V_g, it was possible to collect both fast H^- ions and the low-energy collision products (electrons, and for O_2 targets, negative ions as well) at the rear collector R, but only the low-energy collision products at collector F. The difference between these signals gives a measure of σ_{0-1}.

For the results presented here, the H^--production rate is generally small compared to the low-energy negative-charge-production rate, resulting in σ_{0-1} data with considerable statistical scatter. In addition, the procedure is strictly valid only for forward-scattered H^-. Even though Fleischmann, Barnett, and Ray[11] have shown that $d\sigma_{0-1}/d\Omega$ cross sections are much more forward peaked in the low-keV energy range than their $d\sigma_{01}/d\Omega$ counterparts, there is bound to be considerable angular scattering in the region below a few hundred eV, resulting in σ_{0-1} measurements which fall below the true values. This problem will be discussed in more detail when the σ_{0-1} results are presented.

III. DIFFERENTIAL PROTON-PRODUCTION CROSS SECTIONS

As noted in Sec. II, full utilization of the information contained in the signal measurements to collectors A–D (see Fig. 1) requires a knowledge of the angular dependence of the differential proton-production cross section $d\sigma_{01}/d\Omega$. The scattering angles of interest range from about 5° to essentially 180°. For such large angles and over most of the energy range covered, classical cross-section calculations are valid, at least to establish the overall trend of the cross sections. Moreover, these large-angle-scattering collisions are rather hard interactions, occurring at small impact parameters. Accordingly, it was postulated that the angular distribution (though not the absolute magnitude) of the required $d\sigma_{01}/d\Omega$ should be similar to that of the elastic differential-scattering cross section $d\sigma_e/d\Omega$. Evidence to support this postulate will be presented later.

Using a procedure proposed by Dose,[12] and followed in the earlier work on argon targets,[2] the interaction was taken to be

$$U(r) = \int d\tau\, \rho_H(\vec{r}_2) V(r_1)\,, \tag{6}$$

where $\rho_H(\vec{r}_2)$ is the hydrogen-atom charge distribution [a point proton nucleus and the square of the H(1s) electronic wave function] and $V(r_1)$ is the target-particle potential. For the case of argon targets, this target potential was taken to be

$$V(r_1) = \frac{e}{r_1} \sum_n \alpha_n \exp\left(-\frac{r_1}{a_n}\right), \tag{7}$$

as proposed by Smith, Marchi, Aberth, Lorents, and Heinz.[13] Here, the sum ranges over the K, L, and M shells ($\alpha_n = 2, 8, 8$, respectively), and the screening lengths a_n(0.057, 0.18, and 0.93 bohr) were determined from $a_n = (I_H/I_n)^{1/2} a_0$, where I_H is the atomic-hydrogen ionization energy and I_n is the ionization energy for the nth argon electronic shell. This potential was convenient as it led to an analytic expression for the interaction, thus facilitating a calculation of the scattering angle versus impact parameter and then $d\sigma_e/d\Omega$.

For the case of molecular targets, however, any detailed formulation of target potential is very complicated and leads to a complex interaction. Yet, the numerous required differential cross sections must encompass wide ranges in both angle and energy, necessitating a simple model and fast calculations.

In view of this situation, it was decided to keep a modification of the Smith *et al.*[13] potential of Eq. (7) for the case of the molecular targets of interest here. So far as the kinematics and maximum nuclear charge of the scattering target are concerned, the target should resemble a "free" nitrogen (or oxygen) atom. Indeed, the large-angle-scattering involved here requires very small impact parameters with the scattering coming effectively from only one of the nuclei, shielded by only a few of its innermost electrons. On the other hand, for smaller scattering angles

TABLE I. Differential proton-production cross section for H+N_2 collisions. H-atom energies are in keV, scattering angles are in the laboratory frame, and cross-section values are in cm^2/sr. The normalization R is $R=(d\sigma_{01}/d\Omega)/(d\sigma_e/d\Omega)$.

θ \ E	0.125	0.25	0.50	1.0	2.0
1.9°	4.7E−16	1.5E−15	3.4E−15	5.4E−15	7.4E−15
4.7°	9.8E−17	2.7E−16	5.0E−16	6.5E−16	7.1E−16
9.3°	2.6E−17	6.2E−17	9.8E−17	1.1E−16	9.6E−17
18.7°	6.1E−18	1.2E−17	1.6E−17	1.4E−17	1.0E−17
42.2°	8.8E−19	1.4E−18	1.4E−18	1.0E−18	6.3E−19
85.8°	1.5E−19	1.9E−19	1.7E−19	1.1E−19	5.7E−20
131.9°	5.9E−20	7.2E−20	5.9E−20	3.5E−20	1.8E−20
R	0.034	0.092	0.190	0.322	0.534

or near the lower end of the energy range covered here, much more Coulomb screening of the nuclei is required, and this screening should look like that provided by the molecular electronic charge distribution.

The N_2 targets were thus taken to be two nitrogen-like atoms, each with the nuclear charge and mass of ordinary nitrogen atoms, but with electronic shells and ionization energies corresponding to the N_2 molecular orbitals $(1\sigma_g)$, $(1\sigma_u)$, $(2\sigma_g)$, $(2\sigma_u)$, $(1\pi_u)^2$, $(3\sigma_g)$. The screening lengths a_n in Eq. (7) were computed from the ionization energies for these orbitals, with the values 409.5, 409.5, 37.3, 18.7, 16.7, and 15.7 eV, respectively.[14]

For O_2 targets, the ionization energies 532.0, 532.0, 42.1, 24.6, 20.3, 18.2, 17.1, 16.1, and 12.1 eV were used corresponding to the orbitals $(1\sigma_g)$, $(1\sigma_u)$, $(2\sigma_g)$, $(2\sigma_u)$, $(3\sigma_g)$, $(1\pi_u)^2$, $(1\pi_g)$, respectively.[15] Two energies (20.3 and 18.2 eV) were assigned, each to a "half" electron in the $(3\sigma_g)$ orbital, to represent the influence of the two ionic states formed when this electron is removed, and different energies (17.1 and 16.1 eV) assigned to the two $(1\pi_u)$ electrons.

The use of the hybrid atomic scattering potential described above thus allows the scattering from molecular targets to be handled in the same way as that from Ar targets described earlier.[2] The computed $d\sigma_e/d\Omega$ cross sections were then used in place of $d\sigma_{01}/d\Omega$ to carry out the integrals of the type in the last term of Eq. (5). By combining the measured signals to the four collectors and these calculations, which give the relative amount of proton scattering to the various collectors, it is possible to "normalize" the magnitude of the computed $d\sigma_e/d\Omega$ (downward) to give the required $d\sigma_{01}/d\Omega$.

The absolute values of the resulting differential proton-production cross section for N_2 and O_2 targets are presented for a range of energies and angles[16] in Tables I and II, respectively. The values of the normalization factor R (the reduction factor by which the computed $d\sigma_e/d\Omega$ must be multiplied to yield the desired $d\sigma_{01}/d\Omega$) are also given.

Note that $d\sigma_{01}/d\Omega$ for N_2 is typically 10% to 20% above that for O_2 at comparable energy and scattering angle. This occurs even though the computed $d\sigma_e/d\Omega$ is larger for O_2 (because of its greater mass and charge). The normalization factor R for O_2 therefore is smaller. It is worth noting that the total proton-production cross section σ_{01} (to be given in Sec. IV) is also about this much larger for N_2 than for O_2. Thus, the higher efficiency for this process in N_2 appears to be independent of the proton scattering angle.

TABLE II. Differential proton-production cross section for H+O_2 collisions. (For definitions, see heading of Table I.)

θ \ E	0.125	0.25	0.50	1.0	2.0
1.9°	3.9E−16	1.2E−15	2.6E−15	4.2E−15	6.0E−15
4.7°	8.3E−17	2.3E−16	4.0E−16	5.3E−16	6.1E−16
9.4°	2.3E−17	5.4E−17	8.2E−17	9.0E−17	8.4E−17
18.8°	5.5E−18	1.1E−17	1.4E−17	1.2E−17	9.4E−18
42.6°	8.3E−19	1.3E−18	1.3E−18	9.3E−19	5.8E−19
86.4°	1.5E−19	1.9E−19	1.6E−19	9.7E−20	5.4E−20
131.9°	6.0E−20	7.2E−20	5.6E−20	3.3E−20	1.8E−20
R	0.029	0.077	0.149	0.244	0.411

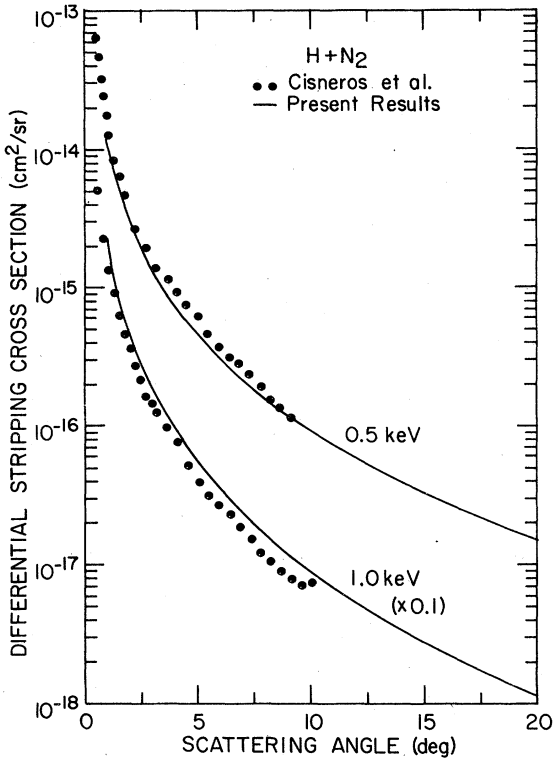

FIG. 2. $H+N_2$ differential proton-production cross sections ($d\sigma_{01}/d\Omega$) at 0.5 and 1.0 keV hydrogen-atom energy. The present results are compared with those of Cisneros *et al.* (Ref. 17) on an absolute basis.

Note also that at the smaller scattering angles, the $d\sigma_{01}/d\Omega$ values tend to increase with increasing energy in much the same way as the corresponding σ_{01} (see Fig. 8 and 9 in Sec. IV). On the other hand, at large angles, the $d\sigma_{01}/d\Omega$ clearly exhibit maxima as a function of energy and appear to be approaching an inverse energy dependence (for fixed large angle) at the higher energies.

In view of the interplay between experiment and calculation used to obtain these results for $d\sigma_{01}/d\Omega$ and the wide ranges of energy and angle covered, it is difficult here to make as definitive an uncertainty analysis as given in the next section for the total cross-section measurements. For energies between 0.25 and 1.0 keV for N_2 targets, for example, where the signals to the various collectors differ by 10% to 30% [i.e., the second term of Eq. (5) is a substantial part of the total signal], the results for $d\sigma_{01}/d\Omega$ should be reliable to ± 25% in the angular range between about 2° and 45°. For O_2 targets, the scattered proton signal is much smaller relative to $S_{O_2^+}$ and the uncertainties are perhaps twice as large in the same energy/angle region. At 2 keV, the scattered proton signals are very small for both N_2 and O_2 targets, and the differential cross sections are more uncertain, as they are at scattering angles above about 45° at all energies. Nevertheless, it is difficult to see how the results could be off by more than about a factor of 2 for the conditions listed.

For the case of N_2 targets, the smaller-angle results obtained here for $d\sigma_{01}/d\Omega$ can be compared with the measured data of Cisneros, Alvarez, Barnett, and Ray.[17] Two such comparisons, at 0.5 and 1.0 keV, are shown in Fig. 2.

Note the rather good agreement between the angular distributions of the two sets of results. Since the present $d\sigma_{01}/d\Omega$ has the angular distribution of the computed $d\sigma_e/d\Omega$, it indeed appears that these cross sections have similar angular dependences, supporting the postulate made earlier.

At 0.5 keV, the measured $d\sigma_{01}/d\Omega$ results of Cisneros *et al.* are typically 20% to 40% above the present data. While this agreement is within the combined uncertainty of the determinations, the present authors feel that the Cisneros *et al.* results are high. Their total σ_{01}, which they obtain by direct integration of the $d\sigma_{01}/d\Omega$ shown in Fig. 2, lies about 40% above the σ_{01} determined here and is even about 25% above the total charge-production cross sections of both Fleischmann and Young[18] and the present σ_t^- and σ_t^+ data.

At 1 keV, the situation is reversed; i.e., the data of Cisneros *et al.* fall 20% to 40% below the present results. Again, this shift is similar to that for the ratios of the total σ_{01} cross sections. As at 0.5 keV, however, the two sets of results fall within mutual uncertainty.

At 2 keV, the Cisneros *et al.* results for $d\sigma_{01}/d\Omega$ are only about 50% of the present results. Unfortunately, however, the present results at 2 keV are also somewhat more uncertain (as discussed above) and the data sets are thus not in conflict.

For O_2 targets, the authors are not aware of any absolute $d\sigma_{01}/d\Omega$ data with which to compare the present results. On the other hand, the angular dependence of the present results agree well with the relative angular distribution measurements of Fleischmann, Barnett, and Ray[11] out to 7° (their largest angle), and the authors can find no reason to suggest that the method might be less satisfactory for O_2 targets.

IV. TOTAL CHARGE-PRODUCTION CROSS SECTIONS

In this section, the results of the measurements for the σ_t^-, σ_t^+, $\sigma_{N_2^+}$, $\sigma_{O_2^+}$, σ_{01}, and σ_{0-1} cross sections are given and compared, where possible, with the data of other investigators. The data are

presented in graphs of cross section versus laboratory hydrogen-atom energy. While the present measurements extend up to 3 keV energy only, the graphs shown include results up to 30 keV, so that better comparisons with other work can be made. The present results are shown as solid data points with solid lines through the points, and the results of other investigators are displayed by open symbols and broken curves.

A. σ_t^- and σ_t^+ cross sections

The total charge-production cross sections σ_t^- and σ_t^+ for N_2 and O_2 targets are presented in Figs. 3 and 4, respectively. In general, the present data lie about 10% to 25% above the results of Fleischmann and Young, [18] within combined uncertainties. While the present results agree well with those of McNeal and Clark[19] for N_2 targets, the present data are about 30% above McNeal, Clark, and Klingberg[20] for O_2 targets, marginally at the limits of the combined uncertainty. It also appears that the present cross section for N_2 could be smoothly extrapolated onto the higher energy data of Solov'ev, Il'in, Oparin, and Fedorenko.[21]

The present data points in the region below 1 keV show alternately the results of the σ_t^- and σ_t^+ measurements. As can be seen, these independent measurements of the same cross section agree well even though they were made under quite different experimental conditions.

This agreement, however, would not have been

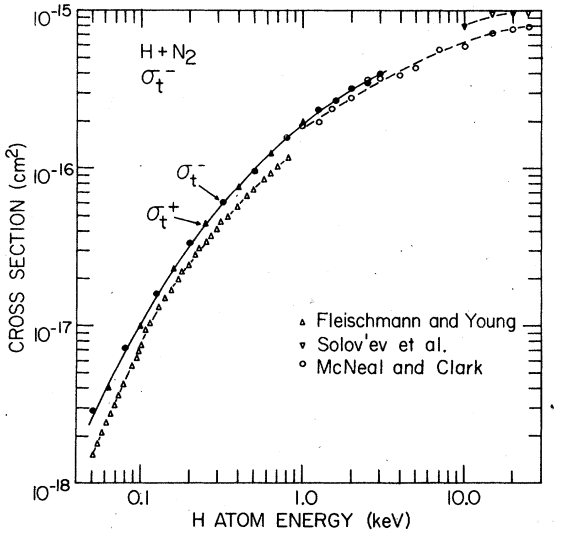

FIG. 3. Total charge-production cross sections for H+N_2 collisions. Solid circles and triangles are present results. Other data are from Fleischmann and Young (Ref. 18), Solov'ev *et al.* (Ref. 21), and McNeal and Clark (Ref. 19).

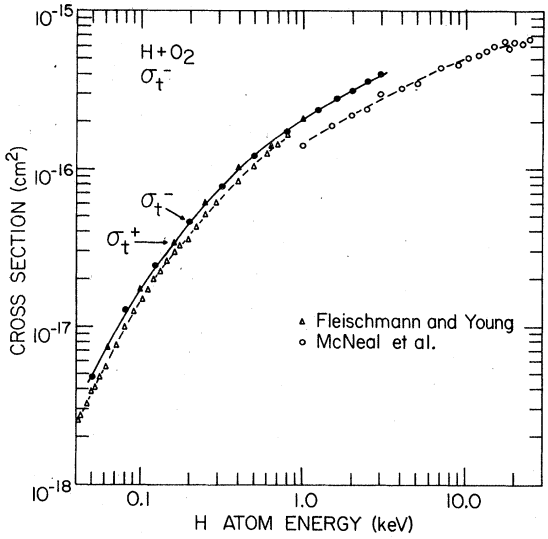

FIG. 4. Total charge-production cross sections for H+O_2 collisions. Solid circles and triangles are present results. Other data are from Fleischmann and Young (Ref. 18) and McNeal *et al.* (Ref. 20).

quite as good if the raw negative-charge signal (in the σ_t^- measurement) had not been corrected for the effect of scattered protons on negative-charge collection. That is, an expression like Eq. (5), except that the sign of the last term is now negative, can be written to express the decrease in negative-charge signal recorded owing to the arrival of scattered protons at the negative-charge collectors. This contribution could now be determined since the required $d\sigma_{01}/d\Omega$ was available from the positive-charge collection studies. While the effect was small, not exceeding 5% for these targets, it can explain some of the increased magnitude of the present σ_t^- over those of previous investigations.

In the earlier paper on argon targets, [1] a detailed discussion of the total-uncertainty analysis was given. Since the uncertainties in the present results are similar, the discussion will not be repeated at length. In summary, the analysis treats both systematic and statistical uncertainties as random, and they are combined in quadrature. The final claimed uncertainty is estimated to be at approximately the 90% confidence level.

For the total charge-production cross sections under consideration here, the total uncertainty is found to be ±12%, except in the region below 100 eV, where it increases to ±25% at 50 eV.

B. $\sigma_{N_2^+}$ and $\sigma_{O_2^+}$ cross sections

The cross sections for target-molecule ionization (which includes dissociative ionization, as discussed in Sec. I), are shown in Figs. 5 and 6.

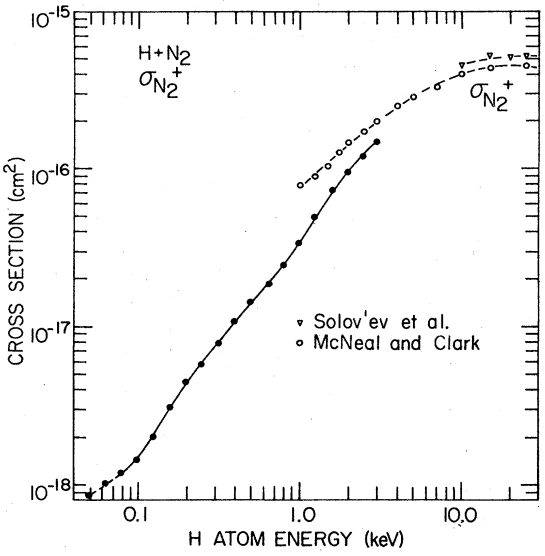

FIG. 5. Total target-ionization cross sections for $H+N_2$ collisions. Solid circles are present results. Other data are from Solov'ev *et al.* (Ref. 21) and McNeal and Clark (Ref. 19).

The results of Solov'ev *et al.* and of McNeal and Clark for N_2 targets and of McNeal *et al.* for O_2 targets are shown for comparison.

In general, the present data fall below those of McNeal and Clark and of McNeal *et al.* and tend to be falling faster with decreasing energy than the results of these other investigators. The present authors attribute this difference to secondary electron problems present in the earlier measurements. In the present research, it was found necessary to collect the slow-ion products from such collisions at collectors (i.e., *A*, *B*, etc.) situated behind the highly transparent grid (see Fig. 1) in order to properly suppress secondary electrons. Such precautions were not taken in the earlier studies.[22] Furthermore, since the source of these secondary electrons is primarily the impact of large-angle-scattered, fast protons and hydrogen atoms impacting the collector surfaces, the problem becomes less important at the higher energies where such scattering is smaller.[23] Thus, at energies much above 3 keV, the earlier measured cross sections should be largely free from this problem.

In the energy region below 80 eV, the target-molecule-ionization cross sections are shown as dashed lines because of the significant uncertainty present here in unfolding the scattered proton contributions to the total positive-ion signal. Nevertheless, the authors believe that the upward tendency of $\sigma_{N_2^+}$ in this region is physically real and suggests the proper trend of this cross section at the very low energies. This trend will be considered later in more detail.

The uncertainties in these cross sections are judged to be ±12% at 3 keV, ±15% at 0.5 keV, ±18% at 0.1 keV, and increase rapidly to about ±30% at 50 eV. Uncertainties at other energies can be obtained by interpolation on a logarithimic energy scale.

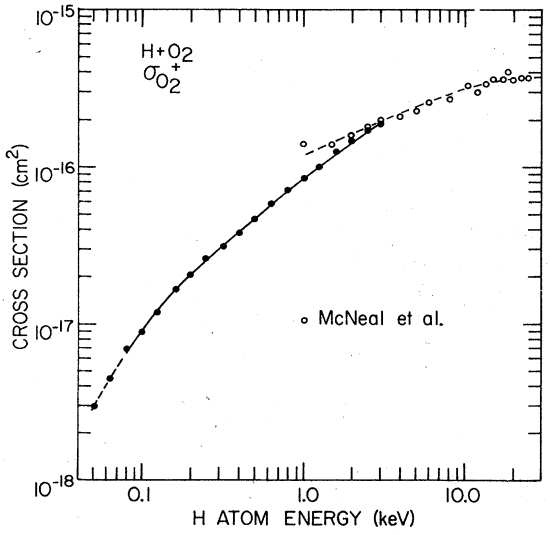

FIG. 6. Total target-ionization cross sections for $H+O_2$ collisions. Solid circles are present results. Other data are from McNeal *et al.* (Ref. 20).

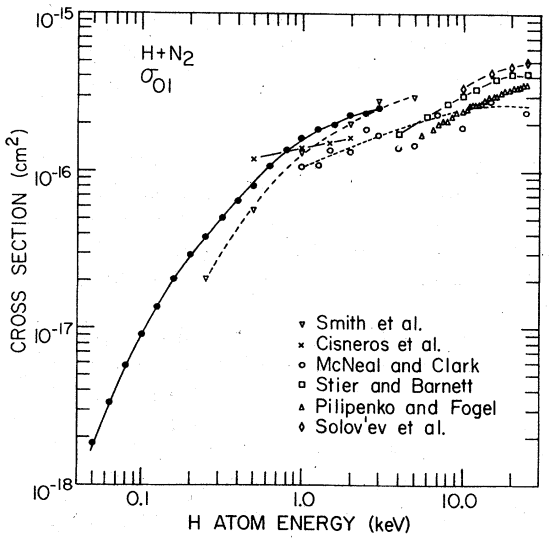

FIG. 7. Total proton-production cross sections for $H+N_2$ collisions. Solid circles are present results. Other data are from Smith *et al.* (Ref. 24), Cisneros *et al.* (Ref. 17), McNeal and Clark (Ref. 19), Stier and Barnett (Ref. 25), Pilipenko and Fogel (Ref. 26), and Solov'ev *et al.* (Ref. 21).

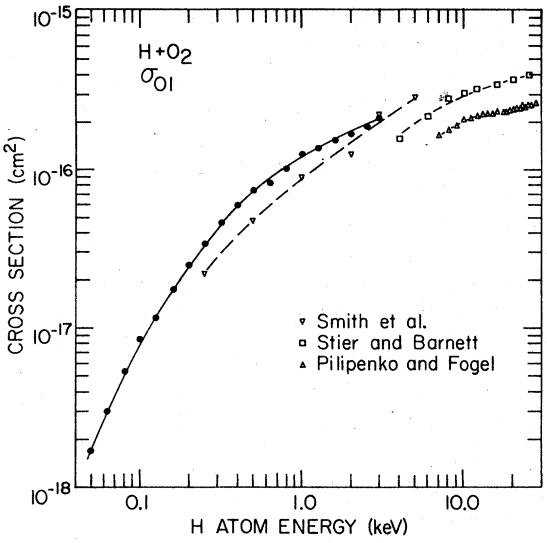

FIG. 8. Total proton-production cross sections for H+O$_2$ collisions. Solid circles are present results. Other data are from Smith *et al.* (Ref. 24), Stier and Barnett (Ref. 25), and Pilipenko and Fogel (Ref. 26).

C. σ_{01} cross sections

Because of the substantial amount of angular scattering which may accompany the production of a proton in a hydrogen-atom collision with a much heavier target in the 100 eV range, no attempt was made to observe directly the protons produced in these reactions. Rather, the proton-production cross section was determined by subtracting the measured target ionization cross section from the measured total charge-production cross section:

$$\sigma_{01}=\sigma_t^- - \sigma_{N_2^+}. \tag{8}$$

This procedure, used previously by McNeal and Clark for H+N$_2$ collisions at higher energies, was felt to be superior in terms of dealing with the proton scattering effect and was also much easier to accomplish in the present experimental apparatus.

The σ_{01} cross sections for N$_2$ and O$_2$ targets determined by the above procedure are presented in Figs. 7 and 8, respectively. The results of Smith, Duncan, Geis, and Rundel[24]; Stier and Barnett[25]; and Pilipenko and Fogel[26] for both targets are also shown, as are the data of Cisneros *et al.*; McNeal and Clark; and Solov'ev *et al.* for N$_2$ only.

Consider first the N$_2$ target data of Fig. 7. In the 2 to 3 keV region the present results and those of Smith *et al.*[24] tend to be about twice as large as the general grouping of the higher-energy data. The data of McNeal and Clark, taken with basically the same techniques used here, are about 40% below the present results, primarily because their σ_t^- is smaller and their $\sigma_{N_2^+}$ is larger.

As noted in Sec. III, the present authors feel that the 0.5-keV point of Cisneros *et al.* is high, as it falls 25% above the total charge-production cross section σ_t^- at this energy. On the other hand, Cisneros *et al.* have also measured σ_{01} for D+N$_2$ collisions. Their value at about 4.1 keV, where the deuterium atom has about the same velocity as a 2-keV hydrogen atom, is somewhat larger than the 2-keV hydrogen atom value and is thus in much better agreement with the present results in the 2-keV region.

The present results are in good agreement with those of Smith *et al.*[24] in the 2-keV region. At lower energies, however, their cross section begins to fall more rapidly than that reported here and is only 55% of the present result at 250 eV, about 15% outside the combined uncertainty.

For O$_2$ targets, the situation is rather similar. The present results are above the higher-energy data of Stier and Barnett and of Pilipenko and Fogel, but agree with the results of Smith *et al.*[24] at the higher energies. Note again, however, the increased divergence of the Smith *et al.*[24] and the present results with decreasing energy.

The fact that this divergence, for both N$_2$ and O$_2$ targets, increases approximately with inverse energy is suggestive that the difference is somehow associated with an angular scattering process. While the Smith *et al.*[24] experiment was of the "cell transmission type" (where a beam of hydrogen atoms enters a suitable target-gas cell and the emergent protons are observed), they were careful to keep their "proton scattering acceptance angle" up to about 15°, and they employed a wide-mouthed Faraday-cup proton collector beyond the target cell. Various experimental tests led them to believe that they were collecting virtually all the scattered protons.

Yet, when the results of Smith *et al.*[24] and the present results[27] are compared for H$_2$ targets, the agreement is excellent over the entire energy range of overlap. For this low-Z small-mass target, of course, the angular scattering is much reduced. In addition, for He targets,[27] while a slight divergence between the two sets of results may occur at the lower energies, the data are quite close and fall well within their mutual uncertainty.

The uncertainties claimed for the present σ_{01} results for N$_2$ targets are ±20% at 3 keV, ±15% between 2 and 0.1 keV, and increase to ±40% at 50 eV. For O$_2$, the uncertainties are about ±25% between 3 and 0.25 keV, increase to ±31% at 0.1 keV, and to ±89% at 50 eV. These

values are obtained by quadrature combination of the uncertainties in the σ_t^- and $\sigma_{N_2^+}$ or $\sigma_{O_2^+}$ cross sections. Again, the uncertainties at other energies can be obtained by interpolation on a logarithmic energy scale.

D. σ_{0-1} cross sections

The total charged-particle-production cross-section data presented to this point have been of high quality from the viewpoint of minimum uncertainty, high reproducibility, and satisfaction of all the checks and tests to which they were subjected. In sharp contrast, the σ_{0-1} results are not up to these standards. Nevertheless, although they exhibit considerable statistical scatter, as noted in Sec. II, the data are presented here as they do contribute to the understanding of the interactions under study.

The σ_{0-1} results for N_2 targets are shown in Fig. 9, along with the data of Stier and Barnett and of Pilipenko and Fogel at higher energies. The curve for $\sigma_{N_2^+}$ from Fig. 5 is also presented again, as an N_2^+ ion (or dissociation fragment) must be produced along with each H^- formed. The flags shown on some data points are estimates of typical statistical uncertainties present in the measurements (being large, as explained in Sec. II, when the measured signals to collectors *F* and *R* are comparable) and should not be taken as absolute uncertainty limits.

Note first that the results at higher energies, although badly scattered, appear to join smoothly

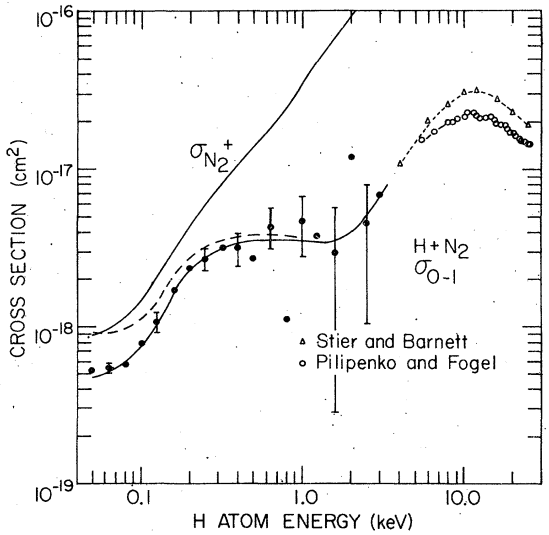

FIG. 9. Total H^--production cross sections for H + N_2 collisions. Solid circles are present results. Other data are from Stier and Barnett (Ref. 25) and Pilipenko and Fogel (Ref. 26).

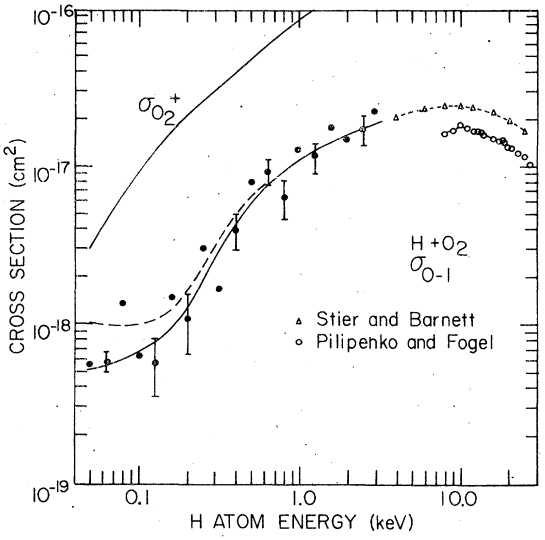

FIG. 10. Total H^--production cross sections for H+O_2 collisions. Solid circles are present results. Other data are from Stier and Barnett (Ref. 25) and Pilipenko and Fogel (Ref. 26).

with the data of the other workers cited. While the scatter is largest here, the method used for the cross-section determination should be reliable, and the trend of the results should be correct.

At the lower energies, on the other hand, the statistical scatter is much diminished but the method of determining σ_{0-1} becomes increasingly inadequate, due to the possibility of angular scattering of the H^- at its time of formation. In the earlier work on argon targets,[1] there was reason to suspect that the measured σ_{0-1} cross section could be low by about a factor of 2 at 50 eV, and at other energies by an amount given approximately by

$$\sigma_{0-1}(\text{true}) = \sigma_{0-1}(\text{measured})\,(1 + 50/E)\,, \qquad (9)$$

where *E* is the hydrogen-atom energy in eV. If such a correction is applied to the present measured σ_{0-1}, the result obtained is indicated by the long-dashed curve in Fig. 9. Note that, at the lowest energies, this σ_{0-1}(true) is comparable in magnitude to $\sigma_{N_2^+}$.

The σ_{0-1} data for O_2 targets are presented in Fig. 10. In general, the agreement with the higher-energy results is good, particularly with those of Stier and Barnett. The long-dashed line at the lower energy is again the result of an application of Eq. (9) to the measured data. Note that in this case, however, the σ_{0-1}(true) falls well below $\sigma_{O_2^+}$. Also note that this occurs because $\sigma_{O_2^+}$ is much larger than $\sigma_{N_2^+}$ at the low energies, not because the σ_{0-1} cross section is

any smaller for O_2 targets.

No detailed uncertainty analysis was undertaken for the σ_{0-1} results, because of the unknown amount of H^- angular scattering taking place during the collisions in which they are formed.[28] On the other hand, if the σ_{0-1}(true) curves are used at the lower energies, the authors would be surprised if the results were to be in error by much more than a factor of 2 in the energy range covered.

V. DISCUSSION OF THE RESULTS

In the earlier studies of H + Ar collisions,[1] the authors were able to discuss possible reactions on the basis of the interaction potential energy curves for the hydrogen-atom–argon-atom system. It was suggested that the $H^- + Ar^+$ ionic state of the system might be readily populated during a collision, as the long-range attraction of this ionic-potential-energy curve causes it to diabatically cross the inherently repulsive H + Ar ground-state curve at low interaction energy (at about 1 Å separation). As these ionic collision products separate, however, this state must cross all possible H* + Ar levels, many of the H + Ar* levels, and finally break into the $H^+ + Ar$ ionization continuum before the separation is complete. At the relatively low collision velocities covered in these studies ($v_H \lesssim 10^8$ cm/sec), outgoing collision products do not always survive in the ionic channel, but may transfer to other system states at the various crossings, the $H^- + Ar^+$ state thereby providing an intermediate mechanism for the reaction process. This suggestion was consistent with (but certainly not proven by) the energy dependences of the cross sections for some excitation and ionization processes cited in that paper.

While the details of the potential-energy surfaces for the H + N_2 interaction are unknown, some very general similarities with Ar targets can be described with a simple binary picture of the collision. The ground state of the H + N_2 system is repulsive. On the other hand, the $H^- + N_2^+$ ionic state will be long-range attractive, with the nature of the positive ion (e.g., whether Ar^+ or N_2^+) having little influence on the potential-energy curve shape for ion separations beyond a few angstroms. If this state is populated during a collision, the outgoing ionic products must again cross such states as H* + N_2, H + N_2*, and $H^+ + N_2$ as the separation proceeds. Furthermore, as Ar^+ and N_2^+ have similar ionization energies, the crossings should occur at very similar separations.

In general, there are many similarities between the total charge-production cross sections for Ar and N_2 targets. The σ_i^- cross sections are everywhere within about a factor of 2 of each other. Below a few keV, the proton-production cross section σ_{01} is well above that for target ionization, except in the very-low-energy region below 100 eV. For Ar targets, a well-defined peak in the σ_{0-1} and σ_{Ar^+} cross sections was found at 70 eV energy with another maximum in σ_{0-1} at about 300 eV. The σ_{0-1} and $\sigma_{N_2^+}$ cross sections of Fig. 9 show similar features, although not quite so pronounced as in the case of Ar. Nevertheless, it appears that the ion-pair-formation reaction may be the most important ion-formation reaction in the region below 50 eV.

As was the case for Ar targets, the σ_{0-1} cross section for N_2 drops rapidly with decreasing energy between 10 and 2 keV. Again this is just the energy range where the cross sections for populating the H* ($n = 2$) states[29] and the H* ($n = 3$) states[30] are increasing with decreasing energy, supporting the suggestion that the ionic state may be feeding these final excited levels.

For O_2 targets, the situation is more complex. Here both the $H^- + O_2^+$ and $H^+ + O_2^-$ states may be candidates for low-interaction-energy diabatic crossings with a repulsive H + O_2 surface. These states are separated by only about 2 eV (at infinity) and are also close to the $H^+ + O_2$ and H + O_2^+ levels. Obviously ample opportunities for multiple crossings exist for this interaction.

The relative magnitudes of the various charge-production cross sections are also different for O_2. For example, the σ_{01} and $\sigma_{O_2^+}$ cross sections have comparable magnitudes in most of the energy range covered, although $\sigma_{O_2^+}$ may be decreasing less rapidly below 100 eV, possibly because the $H^- + O_2^+$ formation is again becoming important at low energies. Unfortunately, the present studies cannot shed light on the possible importance of the $H^+ + O^-_2$ formation process.

For N_2 targets, the first absolute comparison of magnitude of the $d\sigma_{01}/d\Omega$ cross section determined by the techniques outlined in Sec. III with an independent measurement of this differential proton-production cross section is provided by the data of Cisneros *et al.* As can be seen by the data of Fig. 2, the technique appears to be capable of yielding cross sections accurate with respect to both their magnitude and their angular distribution. The hybrid-atom potential used to allow simple calculations with molecular targets seems to be satisfactory. It should be kept in mind, however, that this model is reasonable only for large-angle scattering, small-impact-parameter collisions, as neither inelastic nor charge-polarization effects have been considered.

It is also interesting to note that the angular distribution of the present $d\sigma_{01}/d\Omega$ agrees well

with that measured by Cisneros *et al.* at 0.5 keV (see Fig. 2) even though it was computed for an elastic scattering process. Based on these results for N_2 and O_2 molecules and the earlier studies for Ar targets, it appears that the angular distribution for at least this inelastic process is quite similar to that for elastic scattering at large angles well down into the hundreds of eV energy range.

ACKNOWLEDGMENT

This work was supported by the Atmospheric Sciences Section of the National Science Foundation under Grant No. ATM73-00654.

[1]B. Van Zyl, T. Q. Le, H. Neumann, and R. C. Amme, Phys. Rev. A 15, 1871 (1977).
[2]H. Neumann, T. Q. Le, and B. Van Zyl, Phys. Rev. A 15, 1887 (1977).
[3]Space charge caused the beam to increase to 2 or 3 mm in diameter below 100 eV.
[4]The photodetachment efficiency has an inverse velocity dependence. Beam intensities range between 10^{10} and 10^{11} atoms/sec.
[5]B. Van Zyl, N. G. Utterback, and R. C. Amme, Rev. Sci. Instrum. 47, 814 (1976).
[6]The authors treat systematic uncertainties (instrument calibrations, etc.) and statistical uncertainties (meter readings, etc.) as random. The quoted net uncertainty (i.e., the ±3% for the beam-flux intensity given here) is obtained by quadrature combination of the individual uncertainties and is estimated to be on a par with about 9% or higher confidence limits for the measurements.
[7]S. Ruthberg, J. Vac. Sci. Technol. 6, 401 (1969).
[8]B. Van Zyl, Rev. Sci. Instrum. 47, 1214 (1976).
[9]N. G. Utterback and G. H. Miller, Phys. Rev. 124, 1477 (1961).
[10]Above this energy, the required potentials caused breakdown in the cell.
[11]H. H. Fleischmann, C. F. Barnett, and J. A. Ray, Phys. Rev. A 10, 569 (1974).
[12]V. Dose, Helv. Phys. Acta 41, 261 (1968).
[13]F. T. Smith, R. P. Marchi, W. Aberth, D. C. Lorents, and O. Heinz, Phys. Rev. 161, 31 (1967).
[14]A. Lofthus and P. H. Krupenie, J. Phys. Chem. Ref. Data 6, 113 (1977). Values listed by these authors were derived from optical spectra, except for the $(2\sigma_g)$ energy, which was obtained from x-ray photoelectron spectroscopy.
[15]Values for the $(2\sigma_u)$ and higher orbitals are ion-neutral electronic-term energy differences listed by P. H. Krupenie [J. Phys. Chem. Ref. Data 1, 423 (1972)]. The value for the $(1\sigma_g)$ and $(1\sigma_u)$ orbitals is the x-ray value for the 1*s* atomic oxygen orbital from J. A. Bearden and A. F. Burr [Rev. Mod. Phys. 39, 125 (1967)]. The $(2\sigma_g)$ energy is the Hartree-Fock-Roothaan result of P. E. Cade and A. C. Wahl [At. Data Nucl. Data Tables 13, 339 (1974)] reduced by 2.8 eV, as is required to bring the calculated and measured energies for the $(2\sigma_g)$ orbital of N_2 into agreement.
[16]The angles listed are 2°, 5°, 10°, 20°, 45°, 90°, and 135° in the center-of-mass system.
[17]C. Cisneros, I. Alvarez, C. F. Barnett, and J. A. Ray, Phys. Rev. A 14, 84 (1976).
[18]H. H. Fleischmann and R. A. Young, Phys. Lett. 29A, 287 (1969).
[19]R. J. McNeal and D. C. Clark, J. Geophys. Res. 74, 5065 (1969).
[20]R. J. McNeal, D. C. Clark, and R. A. Klingberg, Phys. Rev. A 2, 131 (1970).
[21]E. S. Solov'ev, R. N. Il'in, V. A. Oparin, and N. V. Fedorenko, Sov. Phys. JETP 15, 459 (1962).
[22]In order to check this explanation, measurements were made with a target-cell arrangement similar to that employed in these earlier studies, and results similar to these earlier data were obtained.
[23]It has been the experience of these authors that such problems generally decrease in magnitude at a rate something like $(\text{energy})^{-1}$. The actual dependence is, of course, very complicated as both the energy dependence of the scattering and both the energy and angular dependence of the secondary electron emission come into play here.
[24]K. A. Smith, M. D. Duncan, M. W. Geis, and R. D. Rundel, J. Geophys. Res. 81, 2231 (1976).
[25]P. M. Stier and C. F. Barnett, Phys. Rev. 103, 896 (1956).
[26]D. V. Pilipenko and Ia. M. Fogel, Sov. Phys. JETP 15, 646 (1962).
[27]The present results for $H+H_2$ and H+He collisions are presently being prepared for publication.
[28]Had time permitted, it would have been possible to employ multiple collectors and, with the aid of suitable calculations, evaluate H^- scattering effects in a way similar to that used here to determine the effects of proton scattering.
[29]J. H. Birely and R. J. McNeal, J. Geophys. Res. 76, 3700 (1971).
[30]R. J. Vidmar, M. S. thesis (University of Alaska, 1974) (unpublished).